Mössbauer study of rare-earth intermetallic compounds $R_3T_{29}Si_4B_{10}$

2000 J. Phys.: Condens. Matter 12 5021

(http://iopscience.iop.org/0953-8984/12/23/310)

J. Phys.: Condens. Matter **12** (2000) 5021–5032. Printed in the UK PII: S0953-8984(00)11011-2

Mössbauer study of rare-earth intermetallic compounds $R_3T_{29}Si_4B_{10}$

Heng Zhang†‖, S J Campbell†, H S Li‡, M Hofmann§ and A V J Edge†

† School of Physics, University College, The University of New South Wales, Australian Defence Force Academy, Canberra, ACT 2600, Australia

‡ School of Physics, The University of New South Wales, Sydney, NSW 2052, Australia

§ HMI Berlin, Abteilung NE, Glienickertr 100, D-14109 Berlin, Germany

Received 14 January 2000

Abstract. A ^{57}Fe Mössbauer study has been conducted on the ^{57}Fe doped novel rare-earth intermetallic compounds $R_3T_{29}Si_4B_{10}$ (R = La, Ce, Pr, Nd, Sm, Gd, Tb, Dy, Ho, Er, Tm and Lu, T = Ni, Co). The ^{57}Fe site assignment has been investigated by ^{57}Fe Mössbauer spectroscopy combined with thermodynamic analysis and crystal field estimation. The investigation demonstrated that ^{57}Fe atoms preferentially occupy the 2c crystallographic site with $\bar{4}m2$ local symmetry in the $R_3T_{29}Si_4B_{10}$ compounds. Sequentially, the 8j1, 8j2 and 8i2 crystallographic sites are the second preferentially occupied and 8i3 and 16 K sites are the third preferential occupancy group of iron atoms. The magnetic hyperfine interaction at 4.2 K demonstrates the effect of a spin-induced Co magnetic moment.

1. Introduction

The ternary rare-earth transition-metal silicides RT_9Si_2 [1, 2] with tetragonal $BaCd_{11}$ structure [3] and borides $RT_{12}B_6$ [4, 5] with rhombohedral $SrNi_{12}B_6$ structure [6] have been investigated extensively for their potential applications and interesting magnetic properties. Recently, a novel series of Nd–T–Si–B (T=Co, Ni) compounds have been discovered [7, 8], which established a link between the ternary silicides and borides. Further studies indicated that the compound has a tetragonal structure with space group $P4/nmm$ [9], and its composition can be described by the stoichiometric formula $Nd_3Ni_{29}Si_4B_{10}$ [10]. Neutron diffraction, combined with a Rietveld refinement study revealed that there are two formula units of $Nd_3Ni_{29}Si_4B_{10}$, 92 atoms, with two sets of rare-earth atomic sites, seven sets of transition-metal atomic sites, one set of silicon sites and four sets of boron sites per unit cell [11]. Further investigation indicated that the $R_3T_{29}M_4B_{10}$ family of compounds can form for R = La, Ce, Pr, Nd, Sm, Gd, Ho, Tb, Er, Tm, Dy, Lu and M=Si, Al, Ge, and are isostructural with $Nd_3Ni_{29}Si_4B_{10}$ [12]. Therefore, a group of quaternary rare-earth intermetallics has been established.

A unique phenomenon was observed for the ^{57}Fe Mössbauer spectra of $Nd_3T_{29}Si_4B_{10}$ phase (T = Ni [8], Co [13, 14]), which exhibited a dominant single line at room temperature. This behaviour seems to be linked with the preferential occupancy of ^{57}Fe atoms at a specific crystallographic site with high local symmetry as there are seven transition-metal sites in the $Nd_3Ni_{29}Si_4B_{10}$ structure [11]. In this paper, the ^{57}Fe site occupancy in $Nd_3T_{29}Si_4B_{10}$ (T = Ni and Co) is first investigated. The study is then extended to the whole $R_3Co_{29}Si_4B_{10}$ series. Subsequently, the magnetic hyperfine interaction is explored via the 4.2 K spectra.

‖ Present address: Institute of Materials Science, University of Connecticut, Storrs, CT 06269-3136, USA.

0953-8984/00/235021+12$30.00

2. Experiment

The $Nd_3Ni_{29}Si_4B_{10}$ and $R_3Co_{29}Si_4B_{10}$ samples were prepared by arc melting high purity elements (> 3 N), followed by annealing in an evacuated quartz tube at 900 °C for one week (the samples were wrapped in a tantalum foil). The ^{57}Fe (0.5 wt%, 97.5% enrichment) doped $Nd_3Ni_{29}Si_4B_{10}$ and $R_3Co_{29}Si_4B_{10}$ (R = La, Ce, Pr, Nd, Sm, Gd, Tb, Dy, Ho, Er, Tm and Lu) samples were prepared from the $Nd_3Ni_{29}Si_4B_{10}$ and $R_3Co_{29}Si_4B_{10}$ ingots, and the preparation followed the same procedure as above.

The structure and characterization of the samples was examined by x-ray diffraction using a Philips diffractometer with Cu Kα radiation. The Mössbauer measurements were carried out at room temperature and 4.2 K using transmission mode with a ^{57}Co**Rh** source. A cryostat was used to control the sample temperature for the 4.2 K measurements. The spectrometer was calibrated using a α-Fe absorber and all isomer shifts presented in this paper are relative to α-Fe. Samples were crushed in an agate mortar and pestle to provide a fine powder, which was then put into an absorber holder. The absorber thickness for each sample was estimated by the method reported by Long *et al* [15]. The Mössbauer spectra were fitted by using the fitting program ISOPSEU adopted from Saarbücken University, Germany, with a pseudo-Lorenzian lineshape incorporated [16, 17]. The fitting was performed using the least squares method and the minimization of the standard χ^2 parameters was carried out with respect to each of the free parameters.

3. Results and discussion

The x-ray diffraction measurements confirmed that both the annealed $Nd_3T_{29}Si_4B_{10}$ and ^{57}Fe doped samples are single phase. The lattice parameters are $a = 11.2329(5)$ Å, $c = 7.8761(4)$ Å for the $Nd_3Ni_{29}Si_4B_{10}$ and $a = 11.2345(5)$ Å, $c = 7.8759(4)$ Å for the ^{57}Fe doped sample; and $a = 11.2413(7)$ Å, $c = 7.8907(6)$ Å for the $Nd_3Co_{29}Si_4B_{10}$ and $a = 11.2453(8)$ Å, $c = 7.8907(8)$ Å for the ^{57}Fe doped sample. Only a slight expansion along the basal plane was observed for the ^{57}Fe doped samples.

3.1. Site assignment for $Nd_3T_{29}Si_4B_{10}$ ($T = Ni$, Co)

3.1.1. Room temperature spectra of $Nd_3T_{29}Si_4B_{10}$. The room temperature Mössbauer spectra for the $Nd_3T_{29}Si_4B_{10}$ compounds are shown in figure 1. The spectrum for the $Nd_3Ni_{29}Si_4B_{10}$ sample comprises predominantly a single line. The isomer shift of 0.192 mm s^{-1} is likely to result from the decrease of the s-electron density due to the shielding effect of the 3d electrons of the Ni atoms surrounding the ^{57}Fe atoms. In addition, a sextet of magnetic hyperfine field 26.0(2) T and relative sub-spectral area ~5% corresponding to a $Ni(Fe)_2B$ impurity [18] was also included. The spectrum of the $Nd_3Co_{29}Si_4B_{10}$ contains a dominant single line with isomer shift 0.127 mm s^{-1}, which is smaller than that of the Ni based compound due to the fewer 3d electrons for Co atoms, thereby leading to the weak shielding effect of 3d electrons. In addition, a set of sextets with magnetic hyperfine field and relative subspectrum area of 30.8(1) T, 5 (4)% due to Co (Fe) [19] was also observed.

Further room temperature spectra were collected with a reduced velocity in order to increase the resolution of the subspectra associated with $Nd_3T_{29}Si_4B_{10}$ (figure 1(b)). The spectra showed the existence with doublets of small subspectral areas. However, the fitting is uncertain as the quadrupole interaction splitting QS parameters are not available for the two options of the two doublets as shown in table 1 (the sextet from impurities has been accounted and the remaining subspectra have been normalized).

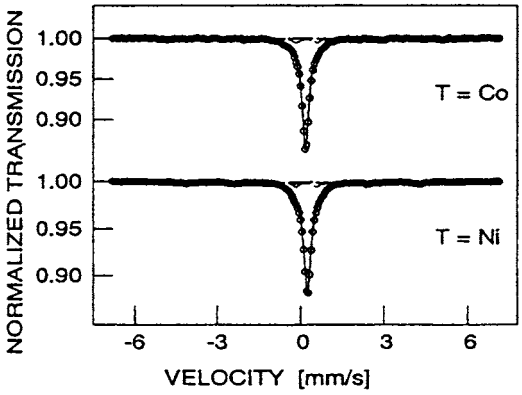

(a)

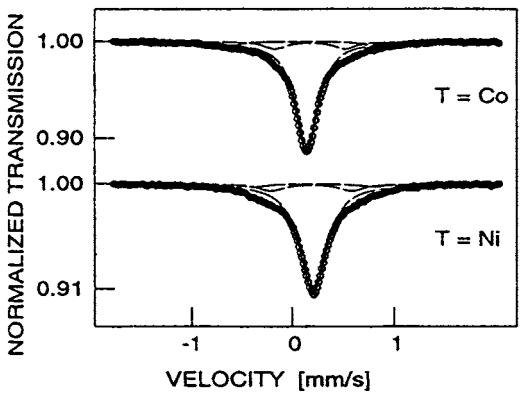

(b)

Figure 1. Mössbauer spectra of $Nd_3T(^{57}Fe)_{29}Si_4B_{10}$ (T = Co, Ni) at room temperature with (a) extended velocity and (b) reduced velocity.

Table 1. Two possible fittings (f1 and f2) of the two doublets for $Nd_3T_{29}Si_4B_{10}$ (figure 1, see text). The brackets after the numerical results indicate the statistical uncertainty in the final digits.

$Nd_3T_{29}Si_4B_{10}$		IS (mm s^{-1})	QS (mm s^{-1})	Γ (mm s^{-1})	Area (%)		IS (mm s^{-1})	QS (mm s^{-1})	Γ (mm s^{-1})	Area (%)
T = Ni	f1	0.195	0	0.31(2)	84(2)	f2	0.195	0	0.31(2)	83(1)
		0.174(9)	0.80(2)	0.32(1)	11(2)		0.12	0.90(1)	0.30(2)	11(3)
		0.20(2)	1.19(3)	0.32(1)	5(3)		0.30(2)	0.94(2)	0.32(1)	6(3)
T = Co	f1	0.131	0	0.27(1)	83(1)	f2	0.131	0	0.270(2)	85(1)
		0.160(5)	0.69(1)	0.26	11(1)		0.22(1)	0.81(1)	0.25	10(2)
		0.08(1)	1.36(1)	0.26	5(1)		0.07(1)	1.04(2)	0.25	5(2)

3.1.2. Thermodynamic estimation for the atomic cluster at transition-metal sites. There are seven transition metal sites for $Nd_3T_{29}Si_4B_{10}$ and the coordination ligands of the nearest neighbours for each site are shown in table 2 [11]. Usually, ^{57}Fe atoms preferentially occupy sites of larger size [20, 21]. From the average atomic distance of the nearest neighbours for the seven Ni sites of $Nd_3Ni_{29}Si_4B_{10}$ structure in table 2, the Ni2 site seems to be the favourable site for occupation by Fe atoms. However, atomic configuration is controlled

Table 2. Coordination ligands and average distance d_{ave} for Ni crystallographic sites in $Nd_3Ni_{29}Si_4B_{10}$ structure.

Atom	Site	Ligand	Number	d_{ave} (Å)	Atom	Site	Ligand	Number	d_{ave} (Å)
Ni1	(2c)	$-Ni^{12}$	(12)	∼2.5491	Ni5	(8j1)	$-NdNi^9Si^2B^2$	(14)	∼2.5636
Ni2	(8i1)	$-Nd^3Ni^6Si^3B$	(13)	∼2.6587	Ni6	(8j2)	$-NdNi^9B^4$	(14)	∼2.4553
Ni3	(8i2)	$-NdNi^9SiB^3$	(14)	∼2.5000	Ni7	(16k)	$-Nd^2Ni^7SiB^3$	(13)	∼2.5295
Ni4	(8i3)	$-Nd^2Ni^7SiB^3$	(13)	∼2.5253					

more by thermodynamics. An atomic configuration with the lowest free energy will be the preferential choice.

Here, we use the Miedema model to estimate the cohesive behaviour of the systems. Miedema's macroscopic atomic model has been used to successfully predict the formation enthalpy of binary crystalline compounds, liquid and solid solution [22, 23]. The enthalpy of formation for an alloy is composed of a negative contribution from the difference between the electronegativities ϕ^* of the two constituent elements, and a positive contribution from the difference between the electron densities n_{ws} at the surface of the Wigner–Seitz cell. The heat of formation can be expressed as [22]:

$$\Delta H^{for} = X_A f_B^A \Delta H^0_{A\ in\ B} = X_A f_B^A 2V_A^{3/2}\{-P[\phi^*_A - \phi^*_B]^2 + Q[(n_{ws}^{1/3})_A - (n_{ws}^{1/3})_B]^2 - R\} \\ /[(n_{ws}^{-1/3})_A + (n_{ws}^{-1/3})_B] \quad (1)$$

where X is the atomic fraction, V the atomic volume, $\Delta H^0_{A\ in\ B}$ the partial molar heat of solution of A in liquid B at infinite dilution, f_B^A the degree by which A atoms are surrounded by neighbours of the other type atoms, B, P, Q, R the related constants, ϕ^* the electronegativity and n_{ws} the electron density at the surface of the Wigner–Seitz cell. It means that the more negative the value of the enthalpy of formation, the stronger the reaction between dissimilar atoms, resulting in a more stable atomic configuration.

The interaction between atoms in a quaternary system is complicated but the enthalpy of formation for related binary systems could be used to estimate the enthalpy and stability for the compound. The enthalpies of formation of relative binary systems calculated with equation (1) and the Miedema parameters [22, 23] are listed in table 3. The enthalpy of formation for Nd–Fe is positive whereas both Nd–Ni and Nd–Co exhibit large negative values. This means that there is strong interaction between the pair of Nd–Ni (Co) atoms, whereas the interaction between the Fe-Nd atoms is weak. The formation of Fe–Nd pairs in a local atomic cluster by substituting for Ni (Co)–Nd pairs will lead to a significant rise in the free energy in the system, therefore formation of Fe–Nd pairs is unfavourable from a thermodynamic viewpoint. Hence, the ^{57}Fe atoms are expected to preferentially occupy the sites with fewest rare-earth atom neighbours. According to the coordinate polyhedral ligands of all the Ni sites of the $Nd_3Ni_{29}Si_4B_{10}$ structure (table 2), the sequence of preferential occupancy of Fe atoms can be classified as

No 1: Ni1 (2c) with 12 Ni (Co) atoms as the ligands
No 2: Ni3 (8i), Ni5 (8j) and Ni6 (8j) with $-NdNi^9B^{4-x}Si^x$ ($x = 0$–2)
No 3: Ni4 (8i) and Ni7 (16k) with $-Nd^2Ni^7SiB^3$ ligands
No 4: Ni2 (8i) with $-Nd^3Ni^6Si^3B$ ligands.

As a first approximation and assuming that the enthalpy of an atomic cluster for a transition metal site is a linear combination of related binary systems of the site centring nearest neighbours, quantitative thermodynamic data can be calculated. We compare the enthalpy of the initial and final atomic configuration after replacement of an Ni (Co) atom by ^{57}Fe for

each site. The enthalpy for each of the transition-metal site clusters for the initial and final configuration after the replacement by a Fe atom can be calculated from:

$$\Delta H = \Delta H_f - \Delta H_i = \frac{1}{n_i}\left(\sum \Delta H_{Fe-i} - \sum \Delta H_{T-i}\right) \tag{2}$$

where ΔH_{Fe-i} and ΔH_{T-i} are the enthalpy for the Fe–i and T–i (T = Ni, Co, and i = Nd, Ni (Co), Si, B binary systems, n_i the ligand number of the i site, respectively. The calculated results are shown in table 4. From the difference of the enthalpy, the preferential site-occupying sequence for Fe is No 1: 2c; No 2: 8j2, 8i2, 8j1; No 3: 16k, 8i3; No 4: 8i1.

Table 3. The calculated enthalpy of formation ΔH^{for}_{A-B} (kJ mol^{-1}) for binary systems based on Miedema parameters [22, 23] and equation (1).

Element	ϕ^* (V)	$n^{1/3}_{ws}$ (du)$^{1/3}$	$V^{2/3}$ (cm^2)
Nd	3.19	1.2	7.51
Ni	5.20	1.75	3.52
Co	5.10	1.75	3.55
Fe	4.93	1.77	3.69
Si	4.70	1.50	4.2
B	5.30	1.75	2.8

ΔH^{for}_{Ni-Nd}	−40	ΔH^{for}_{Fe-Nd}	1	ΔH^{for}_{Co-Nd}	−27
ΔH^{for}_{Ni-Si}	−50	ΔH^{for}_{Fe-Si}	−43	ΔH^{for}_{Co-Si}	−48
ΔH^{for}_{Ni-B}	−33	ΔH^{for}_{Fe-B}	−37	ΔH^{for}_{Co-B}	−34
ΔH^{for}_{Ni-Ni}	0	ΔH^{for}_{Fe-Ni}	−2	ΔH^{for}_{Co-Co}	0
ΔH^{for}_{Fe-Co}	−0.8	ΔH^{for}_{B-Nd}	−55	ΔH^{for}_{Si-Nd}	−57

Table 4. Site atomic cluster thermodynamic estimations for the initial (i) and final (f) configuration after replacement of Ni (Co) by Fe atoms.

Site	Ligands	Enthalpy (i) (kJ mol^{-1})	Enthalpy (f) (kJ mol^{-1})	Difference (average) (kJ mol^{-1})	Order
2c	Co^{12}	0	−0.8	−0.8	1
	Ni^{12}	0	−2	−2	
8i1	$Nd^3Co^6SiB^3$	−17.92	−11.98	5.94	7
	$Nd^3Ni^6SiB^3$	−20.69	−12.54	8.15	
8i2	$NdCo^9SiB^3$	−12.64	−11.44	1.2	3
	$NdNi^9SiB^3$	−13.5	−12.21	1.29	
8i3	$Nd^2Co^7SiB^3$	−15.69	−11.85	3.85	6
	$Nd^2Ni^7SiB^3$	−17.62	−12.77	4.85	
8j1	$NdCo^9Si^2B^2$	−13.64	−11.86	1.79	4
	$NdNi^9Si^2B^2$	−14.71	−12.64	2.07	
8j2	$NdCo^9B^4$	−11.64	−11.01	0.63	2
	$NdNi^9B^4$	−12.29	−11.79	0.5	
16k	$Nd^2Co^7SiB^3$	−15.69	−12.12	3.57	5
	$Nd^2Co^7SiB^3$	−17.62	−13.15	4.46	

The predominant single line at room temperature clearly corresponds to ^{57}Fe atoms located at the 2c site, as the enthalpy decreases for the atomic cluster after the substitution of Co (Ni) atoms by Fe atoms. Combining the Mössbauer spectrum fit results (table 1) with the above analysis, the doublet with the higher fractional area (figure 1(b)) is attributed to the occupancy

of Fe at the sites of group 2: 8j1, 8j2 and 8i2, and the subspectrum with the lower fractional area corresponds to sites of the group 3: 8i3 and 16k. In fact, the 8i1 site is the least favourable site to be occupied by Fe as it results in a significant increase of the enthalpy of the site atomic cluster (table 4).

3.1.3. Quadrupole splitting calculation. Referring to the two possible assignments for the fits of the doublets of the Mössbauer spectra in table 1, we need quadrupole interaction splitting parameters from crystal electric field effects to clarify the site assignment. Further evidence about the site assignment can be estimated from the quadrupole splitting of the Mössbauer spectrum at room temperature.

In the case where the nucleus is not spherical and its charge distribution is not uniform, the interaction of non-cubic extranuclear electric fields with the nuclear charge density results in a splitting of the nuclear energy levels. The interaction of the nuclear electric quadrupole moment eQ with the principal component of the diagonalized electric field gradient (EFG) tensor $V_{zz} = \partial^2/\partial z^2$ at the site of the nucleus splits the nuclear state into sublevels with the eigenvalues in the absence of an internal magnetic field [24]:

$$E_Q = \frac{eQV_{zz}}{4I(2I-1)}\left[3m_I^2 - I(I+1)\right]\left[1+\frac{\eta^2}{3}\right]^{1/2}. \tag{3}$$

The asymmetry parameter η is given by

$$\eta = \frac{V_{xx} - V_{yy}}{V_{zz}} \tag{4}$$

where V_{xx}, V_{yy} and V_{zz} are the non-zero EFG tensor components expressed with respect to the principal axes. Assuming the valence contribution is small for all Ni (Co) sites, and after accounting for the antishielding factor $(1 - r_\infty)$, then the quadrupole splitting from the lattice contribution, which is the variable part due to different site environments, can be expressed as:

$$QS^{lat} = \frac{1}{2}e^2Qq(1-r_\infty)\left(1+\frac{\eta^2}{3}\right)^{1/2} \tag{5}$$

where the antishielding factor is $\sim$10 for ^{57}Fe, $eq = V_{zz}$ is the negative maximum value of the Z component of the electronic field gradient due to the lattice contribution.

The lattice contributions to the crystal field interaction can be evaluated according to a point charge model (PCM) approximation. In the PCM calculation of the lattice contribution to the electric field gradient (EFG), the charge value $+e$ for Nd, $-e/6$ for Co, Ni and Si, and $-e/3$ for B from the empirical values [25], are taken as being located at each atomic position in the $Nd_3Ni(Co)_{29}Si_4B_{10}$ compound, producing electronic field components:

$$V_{ij} = \sum\sum \frac{q_k}{4\pi\varepsilon_0}\left(\frac{3x_ix_j - \delta_{ij}r^2}{r^5}\right) \tag{6}$$

where x, y and z are the components of the position coordinate, $r = (x^2+y^2+z^2)^{1/2}$, the first summation is with respect to different values of the charge q_K, and the second with respect to different coordinates.

By summing all the contributions from the surrounding point charge within a sphere of a radius 20 times the lattice parameters, a convergence of better than 1% was obtained. Then, introducing the deduced diagonal tensor value from equation (6) to equation (5), the calculated quadrupole splitting values are obtained and the results are listed in table 5.

The calculated values, together with the fit data in table 5, give a clear indication of site assignment. Firstly, the calculated QS of the 2c site is only 0.017 mm s^{-1} for $Nd_3Ni_{29}Si_4B_{10}$

Table 5. The theoretical values of EFG and QS parameters from the PCM calculation together with the QS (exp.) fit values from the experimental spectra for $Nd_3T_{29}Si_4B_{10}$ (figure 1).

Site	V_{zz} (10^{21} V m^{-2})	η	QS^{lat} (mm s^{-1})	QS^{lat} (average) (mm s^{-1})	QS(exp.) (mm s^{-1})
$Nd_3Ni_{29}Si_4B_{10}$					
2c	0.0051	0.0027	0.017	0.017	0
8i1	0.165	0.0798	0.516		
8i2	0.162	0.634	0.539		
8i3	0.302	0.0782	0.948		
8j1	0.164	0.840	0.570		
8j2	0.188	0.126	0.590	0.566[a]	0.80(2)
16k	0.319	0.269	1.008	0.978[b]	1.19(3)
$Nd_3Co_{29}Si_4B_{10}$					
2c	0.0039	0.0068	0.012	0.012	0
8i1	0.192	0.0105	0.599		
8i2	0.155	0.699	0.522		
8i3	0.299	0.0728	0.935		
8j1	0.170	0.772	0.583		
8j2	0.191	0.186	0.601	0.569[a]	0.76(2)
16k	0.310	0.277	0.982	0.959[b]	1.34(3)

[a] Average value from 8i2, 8j1 and 8j2.
[b] Average value from 8i3 and 16k.

and 0.012 mm s^{-1} for $Nd_3Co_{29}Si_4B_{10}$, which are both close to zero. This confirms the suggestion that the dominant single line for the room temperature spectrum is attributed to the occupancy of ^{57}Fe atoms at the 2c site. However, the local environment of the 2c site with $\bar{4}m2$ symmetry is a quasi-spherical polyhedron instead of a strict spherical polyhedron. Hence, the single line is actually a doublet with a very small quadrupole splitting value. Secondly, the calculated QS values for the other sites may be classified into two groups: the sites with QS value $\sim$0.6 mm s^{-1}, and those $\sim$1.0 mm s^{-1}. The first group contains 8i1, 8i2, 8j1 and 8j2 with QS value of around 0.6 mm s^{-1}. Based on the thermodynamic study (table 4), the 8i1 site is excluded from this group. Therefore, the first group which includes the 8i2, 8j1 and 8j2 sites is likely to correspond to the main doublet with a QS value of around 0.8 mm s^{-1} with a subspectrum fractional area $\sim$7% for $Nd_3T_{29}Si_4B_{10}$. The second group, which includes 8i3 and 16k sites with calculated QS values $\sim$1.0 mm s^{-1} is associated with the second doublet for the fit of the Mössbauer spectrum with a QS value of about 1.2–1.3 mm s^{-1} with a fractional area $\sim$4% (see table 1). Because there are more Nd atomic neighbours for these sites, the ^{57}Fe occupancy of these sites is less than the first group. Although the calculated values of QS are smaller than those for determined from the spectra fits, the ratio of the QS values indicates that only assignment 1 in table 1 is acceptable.

The above investigations indicate that the site assignment for ^{57}Fe atoms based on the thermodynamic analysis is consistent with the quadrupole splitting estimation via the electric field gradient analysis by a point charge model. However, it cannot further identify the exact site occupancy for each site because the doublets have similar QS values, lower population of Fe atoms and limited resolution of the spectra (figure 1).

3.2. Room temperature spectra fits of $R_3Co_{29}Si_4B_{10}$

The room temperature Mössbauer spectra of all the other $R_3Co_{29}Si_4B_{10}$ compounds exhibit similar characteristics as $Nd_3T_{29}Si_4B_{10}$. According to the above discussion, we apply the

above assignment 1 model to all of the $R_3Co_{29}Si_4B_{10}$ systems. The results of the fits of the room temperature Mössbauer spectra are listed in table 6. The ^{57}Fe occupancies in the three group crystallographic sites are shown in figure 2(a) and the QS values of the two doublets are shown in figure 2(b). The distribution of the site occupancy for the other $R_3Co_{29}Si_4B_{10}$ compounds is similar to that in the $Nd_3T_{29}Si_4B_{10}$.

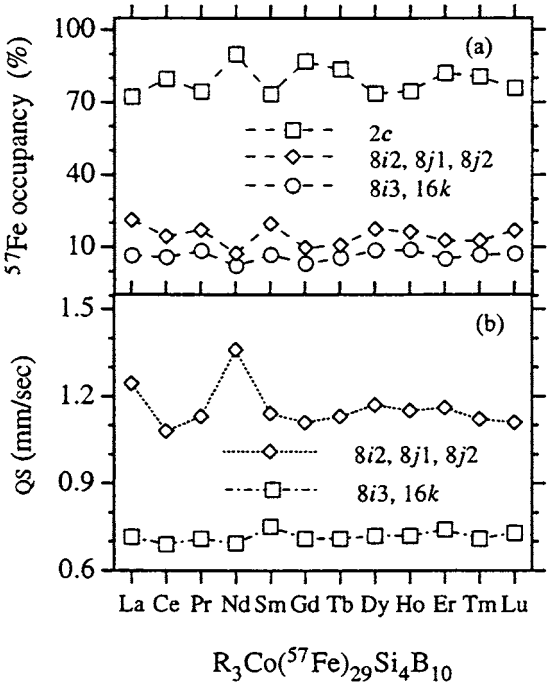

Figure 2. (a) ^{57}Fe site occupancy and (b) quadrupole interaction splitting (QS) of $R_3Co(^{57}Fe)_{29}Si_4B_{10}$ compounds.

3.3. Magnetic hyperfine interaction

The Mössbauer spectra at 4.2 K for the $R_3Co_{29}Si_4B_{10}$ compounds are shown in figure 3. All the spectra contain a dominant sextet with a magnetic hyperfine field ~27 T which corresponds to the ^{57}Fe occupancy at the 2c crystallographic site. Meanwhile, a small fraction of subspectra with a smaller magnetic hyperfine field which are due to the ^{57}Fe occupancy at the other crystallographic sites also exist. As the quadrupole splitting data are not available in the case of magnetic splitting for those sites with minor occupancy, it is impractical to fit these spectra. Here the main effort is focused on the main subspectrum corresponding to the 2c crystallographic site. The magnetic hyperfine fields derived from the fit of the 4.2 K spectra are shown in figure 4. The magnetic hyperfine field increases with the number of unpaired 4f electrons. Two factors may cause the variation of the magnetic hyperfine field versus the atomic number of the rare earth. The first is the size effect due to the lanthanide contraction (which will decrease the distance between the nearest neighbours and the 2c site). The second is the interaction effect of the moment of the rare-earth atoms acting on the central ^{57}Fe atoms at the 2c site. The nearest neighbours to the 2c site are 12 Co atoms, but the second-nearest neighbours comprise two R atoms and eight Co atoms (data calculated from $Nd_3Ni_{29}Si_4B_{10}$

Table 6. The parameters from the fits of the room temperature Mössbauer spectra for $R_3T_{29}Si_4B_{10}$.

	Single line (2c)			Doublet I (8i2, 8j1, 8j2)				Doublet II (8i3, 16 K)			
R	IS (mm s^{-1})	Area (%)	Γ (mm s^{-1})	IS (mm s^{-1})	QS (mm s^{-1})	Area (%)	Γ (mm s^{-1})	IS (mm s^{-1})	QS (mm s^{-1})	Area (%)	Γ (mm s^{-1})
La	0.121(1)	72(1)	0.25(1)	0.162(6)	0.715(8)	20(3)	0.25	0.082(2)	1.244(2)	8(3)	0.25
Ce	0.141(1)	72(1)	0.26(1)	0.151(8)	0.69(1)	16(3)	0.26	0.094(9)	1.08(1)	12(3)	0.26
Pr	0.134(1)	67(2)	0.25(1)	0.157(8)	0.71(1)	21(4)	0.25	0.09(1)	1.13(2)	12(5)	0.25
Nd	0.131(1)	83(1)	0.27(1)	0.160(5)	0693(8)	11(1)	0.26	0.076(9)	1.36(1)	5(1)	0.26
Sm	0.140(1)	68(2)	0.26(1)	0.152(9)	0.731)	20(4)	0.26	0.09(1)	1.14(2)	12(4)	0.26
Gd	0.137(1)	81(1)	0.25(1)	0.158(8)	0.71(1)	12(3)	0.25	0.08(2)	1.11(2)	6(3)	0.25
Tb	0.140(1)	80(1)	0.26(2)	0.139(8)	0.71(1)	13(3)	0.26	0.08(1)	1.13(2)	7(3)	0.26
Dy	0.149(1)	65(3)	0.25(1)	0.149(7)	0.72(1)	22(8)	0.26	0.075(9)	1.17(1)	12(7)	0.26
Ho	0.150(1)	66(3)	0.25(1)	0.149(8)	0.72(2)	20(9)	0.25	0.07(1)	1.15(2)	14(7)	0.25
Er	0.147(1)	75(1)	0.26(1)	0.144(6)	0.74(1)	16(2)	0.26	0.07(1)	1.16(2)	9(3)	0.26
Tm	0.154(1)	71(2)	0.25(1)	0.160(9)	0.71(1)	17(5)	0.25	0.08(1)	1.12(2)	12(5)	0.25
Lu	0.157(1)	70(1)	0.26(1)	0.148(7)	0.73(1)	18(3)	0.26	0.08(1)	1.11(2)	12(4)	0.26
Nd–Ni	0.195(1)	84(1)	0.31(1)	0.174(9)	0.80(2)	11(2)	0.31	0.20(2)	1.11(3)	5(3)	0.31

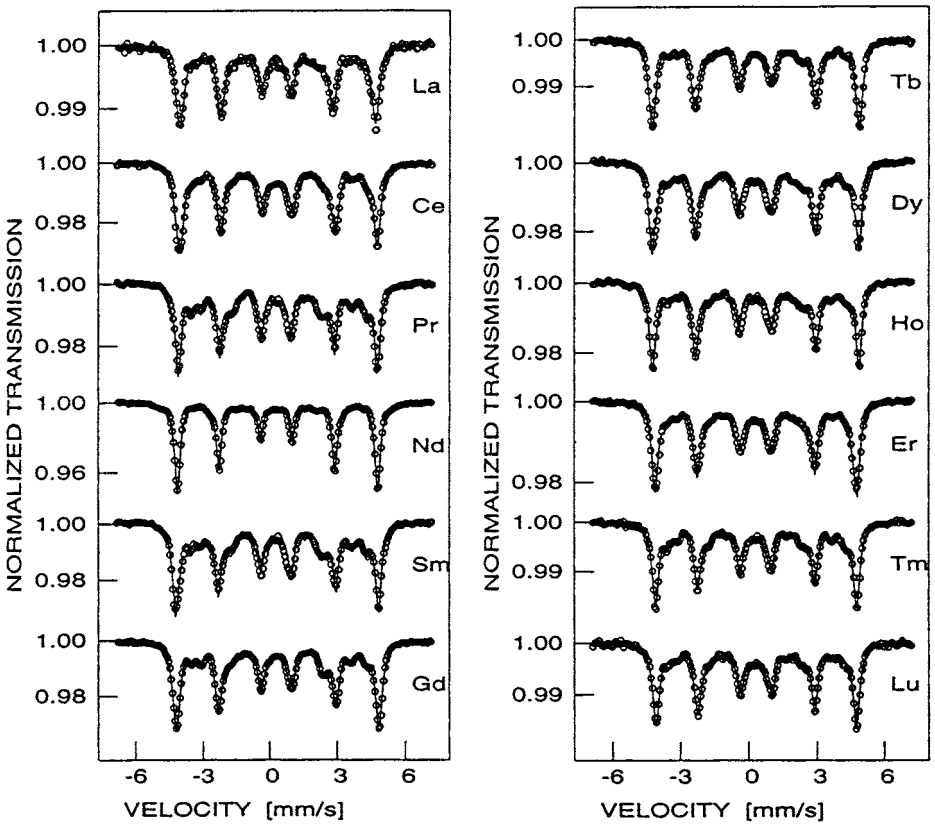

Figure 3. Mössbauer spectra for $R_3Co(^{57}Fe)_{29}Si_4B_{10}$ (a) (R = La, Ce, Pr, Nd, Sm, Gd), and (b) (R = Tb, Dy, Ho, Er, Tm, Lu).

structure). Assuming the size effect on the hyperfine field increases linearly with decrease of unit cell volume (in other words, atomic number), comparing the magnetic hyperfine field values of La and Lu compounds (only size factor acting), the size effect can be removed by a linear subtraction as shown in the dashed line in figure 4. The remaining difference of the hyperfine fields originates mainly from the R–Co interaction, namely the spin-induced Co moment. As shown in figure 4, a stronger effect of R–Co interaction appears for R=Tb, Gd and Dy compounds. This corresponds to the magnetic hyperfine field being proportional to the moment of Co, and, furthermore, the spin-induced Co moment is roughly proportional to the spin moment of the rare-earth ion [26]

$$\langle S_R \rangle = (g-1)\langle J_R \rangle = (g-1)M_R/g \tag{7}$$

where g is the Landé factor, J_R the total angular momentum of the R ion and M_R the magnetic moment of the R ion. The details of R–Co interaction will be further explored elsewhere combining the magnetization and mean molecular field fit. This work is in progress.

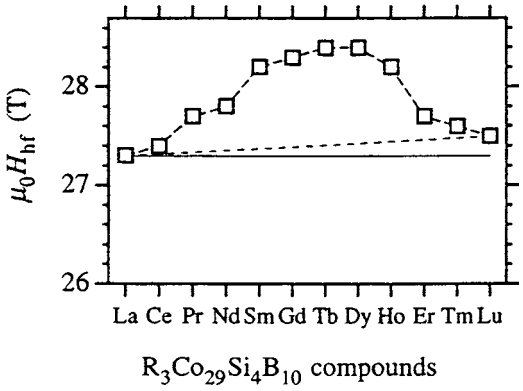

Figure 4. Magnetic hyperfine field derived from the fit of the spectra at 4.2 K of $R_3Co(^{57}Fe)_{29}Si_4B_{10}$ compounds. The gap between the dashed line and solid line represents the effect of unit cell size on the magnetic hyperfine field due to the lanthanide contraction.

4. Conclusion

The ^{57}Fe atom occupancy in the rare-earth transition-metal compounds $Nd_3T_{29}Si_4B_{10}$ has been revealed by the ^{57}Fe Mössbauer spectroscopy measurement combined with thermodynamical analyses and crystal field estimation. The ^{57}Fe Mössbauer spectrum exhibits a dominant single line and a few per cent of two doublets. This behaviour is attributed to the preferential substitution of ^{57}Fe atoms for Ni (Co) atoms at the 2c crystallographic site with $\bar{4}m2$ local symmetry. The other two low percentage doublets result from second and third preferential substitution of ^{57}Fe atoms for Ni (Co) atoms at the group 1, 8i2, 8j1 and 8j2; and group 2: 8i3 and 16k sites. Thermodynamic analyses using the Miedema model indicate that the order of ^{57}Fe occupancy in the $Nd_3T_{29}Si_4B_{10}$ compound follows the lowest free energy of the system. The electronic field gradient estimation by a point charge model has determined uniquely the distribution of the doublets for the Mössbauer experiment.

At 4.2 K, all the spectra contain a dominant sextet with a magnetic hyperfine field $\sim$27.5 T. The deduced magnetic hyperfine field increases with the numbers of unpaired 4f electrons for the $R_3Co_{29}Si_4B_{10}$. This is most likely due to the R–Co interaction, namely the spin-induced Co-moment effect.

Acknowledgments

This work is supported by grants from Australian Research Council, leading to the award of a Postgraduate Research Scholarship (HZ). The project is also partly supported by grants from the Australian Institute of Nuclear Science and Engineering.

References

[1] Malik S K, Zhang L Y, Wallace W E and Sankar S G 1989 *J. Magn. Magn. Mater.* **8** L6
[2] Pourarian F, Malik S K, Boltich E B, Sankar S G and Wallace W E 1989 *IEEE Trans. Magn.* **25** 3315
[3] Bodak O I and Gladyshevskij F J and Dopov 1969 *Akad. Nauk Ukr. RSR* A **5** 452
[4] Jurczky M, Pedziwiatr A T and Wallace W E 1987 *J. Magn. Magn. Mater.* **67** L1
[5] Rosenberg M, Mittag M and Buschow K H J 1988 *J. Appl. Phys.* **63** 3586
[6] Nihara and Yajima S 1972 *Chem. Lett.* 875
[7] Wu E, Wantenaar G H J, Campbell S J and Li H-S 1993 *J. Phys.: Condens. Matter* **5** L4571

[8] Zhang Heng, Campbell S J, Bulcock S, Edge A V J and Wu E 1997 *Physica* B **229** 333
[9] Bulcock S R, Zhang Heng, Wu E and Campbell S J 1998 *J. Mater. Sci. Lett.* **17** 1791
[10] Zhang Heng, Campbell S J, Li H-S and Wu E 1999 *J. Alloys Compounds* **284** 155
[11] Zhang Heng, Campbell S J, Wu E, Kennedy S J, Li Hong-Shuo, Studer A J, Bulcock S R and Rae A D 1998 *J. Alloys Compounds* **278** 239
[12] Zhang Heng, Campbell S J and Edge A V J 2000 *J. Phys.: Condens. Matter* **12** L159
[13] Campbell S J, Zhang Heng, Li Hong-Shuo and Wu E 1998 *J. Magn. Magn. Mater.* **177–81** 1103
[14] Wu E, Zhang Heng and Campbell S J 1998 *Phys. Status Solidi* b **207** 485
[15] Long G J, Granshaw T E and Longworth G 1983 *Möss. Eff. Ref. Data J.* **6** 42
[16] Price D C, Campbell S J and Back P J 1980 *J. Physique Coll.* **41** C1 236
[17] Price D C 1981 *Aust. J. Phys.* **34** 51
[18] Murphy K A and Hershkowitz N 1973 *Phys. Rev.* B **7** 23
[19] Perlow G J, Johnson C E and Mashell W 1965 *Phys. Rev.* A **140** 875
[20] Berthier Y, Chevalier B, Etourneau J, Rechenberg H R and Sanchez J P 1988 *J. Magn. Magn. Mater.* **74** 19
[21] Harker S J, Cardogan J M, Stewart G A, Campbell S J, Kennedy S J and Edge A V J 1998 *J. Magn. Magn. Mater.* **183** 101
[22] Miedema A R, de Chatel P F and de Boer F R 1980 *Physica* B **100** 1
[23] Niessen A K, DeBoer F R, Boom R, de Chatel P F, Mattens W C M and Miedema A R 1983 *CALPHAD* **7** 51
[24] Gonser U 1975 *Mössbauer Spectroscopy* (Berlin: Springer)
[25] Smit H H A, Thiel R C and Buschow K H J 1988 *J. Phys. F: Met. Phys.* **18** 295
[26] Buschow K H J 1971 *Phys. Status Solidi* a **7** 199